Universiteit Antwerpen

This item is the archived peer-reviewed author-version of:

CFD modeling of transient adsorption/desorption behavior in a gas phase photocatalytic fiber reactor

Reference:

Verbruggen Sammy, Keulemans Maarten, van Walsem Jeroen, Tytgat Tom, Lenaerts Silvia, Denys Siegfried.- CFD modeling of transient adsorption/desorption behavior in a gas phase photocatalytic fiber reactor

Chemical engineering journal - ISSN 0300-9467 - (2016), p. 1-35

Full text (Publishers DOI): http://dx.doi.org/doi:10.1016/j.cej.2016.02.014

uantwerpen.be

Institutional repository IRUA

Accepted Manuscript

CFD Modeling of Transient Adsorption/Desorption Behavior in a Gas Phase Photocatalytic Fiber Reactor

Sammy W. Verbruggen, Maarten Keulemans, Jeroen van Walsem, Tom Tytgat, Silvia Lenaerts, Siegfried Denys

PII: S1385-8947(16)30096-1
DOI: http://dx.doi.org/10.1016/j.cej.2016.02.014
Reference: CEJ 14747

To appear in: *Chemical Engineering Journal*

Received Date: 9 October 2015
Revised Date: 31 January 2016
Accepted Date: 5 February 2016

Please cite this article as: S.W. Verbruggen, M. Keulemans, J. van Walsem, T. Tytgat, S. Lenaerts, S. Denys, CFD Modeling of Transient Adsorption/Desorption Behavior in a Gas Phase Photocatalytic Fiber Reactor, *Chemical Engineering Journal* (2016), doi: http://dx.doi.org/10.1016/j.cej.2016.02.014

This is a PDF file of an unedited manuscript that has been accepted for publication. As a service to our customers we are providing this early version of the manuscript. The manuscript will undergo copyediting, typesetting, and review of the resulting proof before it is published in its final form. Please note that during the production process errors may be discovered which could affect the content, and all legal disclaimers that apply to the journal pertain.

ACCEPTED MANUSCRIPT

CFD Modeling of Transient Adsorption/Desorption Behavior in a Gas Phase Photocatalytic Fiber Reactor

Sammy W. Verbruggen[†,‡,§], *Maarten Keulemans*[†,‡,§], *Jeroen van Walsem*[†], *Tom Tytgat*[†], *Silvia Lenaerts*[†], *Siegfried Denys*[†,*]

† Sustainable Energy, Air & Water Technology, Department of Bioscience Engineering, University of Antwerp, Groenenborgerlaan 171, B-2020 Antwerp, Belgium.

* E-mail: Siegfried.Denys@uantwerp.be

Fax: +32 3 265 32 25. Tel: +32 3 265 32 30.

‡ Center for Surface Chemistry and Catalysis, KU Leuven, Kasteelpark Arenberg 23, B-3001 Heverlee (Leuven), Belgium

§ These authors contributed equally

Keywords

Computational Fluid Dynamics (CFD); Adsorption/desorption; Titanium dioxide (TiO2); Fibers; Gas Phase; Acetaldehyde; Kinetic Model; Transient

ACCEPTED MANUSCRIPT

Abstract

We present the use of computational fluid dynamics (CFD) for accurately determining the adsorption parameters of acetaldehyde on photocatalytic fiber filter material, integrated in a continuous flow system. Unlike the traditional analytical analysis based on Langmuir adsorption, not only steady-state situations but also transient phenomena can be accounted for. Air displacement effects in the reactor and gas detection cell are investigated and inherently made part of the model. Incorporation of a surface aldol condensation reaction in the CFD analysis further improves the accuracy of the model which enables to extract precise, intrinsic adsorption parameters for situations in which analytical analysis would otherwise fail.

1. Introduction

Integration or retrofitting of photocatalytic air purifying units into continuous flow systems like HVAC (Heating, Ventilation and Air Conditioning) equipment is an interesting approach for abating indoor air pollution [1–5]. Photocatalytic oxidation (PCO) is an advanced oxidation process (AOP) that is well-suited to fully mineralize gaseous organic contaminants to CO_2 and water using only light as an energy source, as reviewed recently [6]. The possibility of running photocatalytic air purifiers at ambient conditions is an additional asset. Commonly, TiO_2-based materials are used to this end. Due to the often nano-sized dimensions, immobilization of the photocatalyst on a support is key for safeguarding human health [7,8]. Several kinds of substrates have been suggested, ranging from monoliths, over coated plates, slides or cylinders to cloth [9–17]. In one of our previous studies we have demonstrated that a packed bed of TiO_2 coated glass beads around a UV lamp showed high efficiency towards the photocatalytic degradation of ethylene in the gas phase [18]. This was explained by the combined effects of intimate contact between coating and pollutant, a large exposed external surface area and optimal photon utilization by internal reflection on the glass beads and the inner reactor surface. However, such a reactor design is not well suited for integration in HVAC systems, as problems associated with abrasion or noise might be expected in time. An attractive alternative is the use of glass fiber mats. Coating of mats consisting of thin, long fibers not only offers the advantage of exposing a large catalyst surface area, but the open structure also enables sufficient light penetration, experiences only

ACCEPTED MANUSCRIPT

limited pressure drop, allows for silent operation conditions and still exerts sufficient filtering capacity. Therefore coated glass fiber mats is the filter material investigated in this study.

Determining the kinetic parameters of photocatalytic systems is an important step in the development of efficient air purification units for integration in HVAC systems. Calculation of photocatalytic kinetic parameters is amply discussed and relatively 'straightforward' for batch processes [19–22]. It is somewhat more difficult for continuous flow systems, unless steady state conditions are attained. We have shown that in that case both mass-transfer based analytical models, as well as computational fluid dynamics (CFD) can both quite accurately deliver the Langmuir Hinshelwood photocatalytic kinetic parameters [23]. The former has the additional advantage of discriminating between mass-transfer and kinetic reaction control, while the latter enables to calculate the spatial variation of flow rate, reaction rate and pollutant/product concentrations at the catalyst surface. Modelling of pollutant concentrations away from steady state equilibrium is even less forthright. In the case of a photocatalytic filter in HVAC systems, one can imagine the system will go through several series of conditions where only adsorption occurs in dark, until the light source is activated and pollutants are photocatalytically degraded, after which the lamp is again switched off, etc. Since it is a continuous flow system, these transitions do not occur instantaneously, but transient behavior is observed until steady state is obtained under a given set of conditions. In this work we show how CFD enables accurate modelling of the pollutant concentrations in these transient zones in the case of acetaldehyde adsorption on TiO_2 coated glass fiber filters in dark conditions. This results in useful parameters such as the adsorption/desorption rate constants and the maximum adsorptive capacity of the filter. It thus provides vital information for the design and development of photocatalytic air purification units, since adsorption of pollutants is an essential precursory step in photocatalysis. Besides, adsorption occurs in dark as well as in UV light conditions and should therefore be taken into account during all operation steps of a photocatalytic air purification unit. It is thus not our intention to determine photocatalytic kinetic parameters, but to accurately unravel the sole contribution of adsorption/desorption phenomena during transient operation conditions. This will be the cornerstone for future kinetic investigations by providing reliable *a priori* values of adsorbed surface concentrations in each stage of the transient reaction cycle.

2. Experimental details and methodology

2.1 Photocatalytic test reactor and photocatalytic filter

ACCEPTED MANUSCRIPT

The reactor consists of a borosilicate glass tube with an internal diameter of 4.88 cm and a length of 44 cm. Both ends were sealed airtight with a suitable closing mechanism using butyl rubbers. As in previous work, acetaldehyde was used as model compound for indoor air contamination [12,14,23–25]. In short, acetaldehyde (Air Liquide, 1% in N_2) was mixed with clean air (Air Liquide Alphagaz) using mass flow controllers and dosed to the reactor set-up at an inlet concentrations that were varied between 20 and 220 ppmv at a fixed effective total gas flow rate of 400 cm^3 min^{-1}. The concentration of acetaldehyde was monitored on-line using FTIR spectroscopy by means of the IR peak height at 2728 cm^{-1}, corresponding to the ν(C-H) stretch.

The filter material (Profil, 2.PS3"B.050) comprises of a mesh of glass fibers with a thickness of (36 ± 7) µm, determined by at least 30 thickness measurements of different fibers by optical microscopy, and forms a structure with large open pores. A 10 cm long section of this filter was placed symmetrically in the longitudinal center of the reactor, resulting in an average filter density of (10 ± 1) kg m^{-3}. An image of the reactor is presented in Figure 1a.

A 1.5 wt% colloidal TiO_2 suspension (NanoPhos, 1 wt% inorganic SiO_2 binder) was used in this study. This catalyst suspension is commercially available and industrially applied as anti-microbial and self-cleaning coating solution and is therefore well suited to coat the fiber mats for application in HVAC filter systems. The TiO_2 nanoparticles are crystalline with a primary particle size between 18 and 21 nm and consist of a mixed phase of anatase (75%) and rutile (25%).The filters were coated by submersion in the abovementioned TiO_2 suspension and drying at 70 °C overnight. Two coated filters were prepared: a first sample by submersion in the as-received suspension (further denoted as sample A) and a second one by submerging the filter in the colloidal suspension at higher TiO_2 concentration (sample B). The latter suspension was prepared by decanting the original 1.5 wt% suspension and re-suspending the precipitated TiO_2. For correct analysis (see further), reference experiments were also performed using non-coated fiber filters as well as an empty reactor (in which case no fiber filter was used at all).

Before each measurement a 12 hour pretreatment phase was carried out under UV illumination to remove possible organic rest fractions still present on the filter material or originating from the coating procedure. Hereto, a Philips Cleo (25 W) UVA lamp was positioned above and parallel to the reactor housing at a height of 2 cm, resulting in an incident intensity on the fiber filter of 1.5 mW cm^{-2}, as measured by a calibrated intensity meter (Avantes Avaspec-3648). For the adsorption tests discussed here, the measurements of the samples typically consisted of two phases: (1) 10 min gas flow in a by-pass modus during

ACCEPTED MANUSCRIPT

which the reactor was sealed off and (2) 45 min gas flow through the reactor in dark conditions in order to achieve adsorption-desorption equilibrium. Afterwards the lamp was switched on and the contribution of the acetaldehyde adsorption-desorption equilibrium under kinetic operation was further investigated. The impact of the transient acetaldehyde adsorption was of such an extent, that the determination of the actual kinetic reaction parameters turned out to be quite complex and is therefore the subject of ongoing research. Hence, this work strictly focuses on the complex contribution of transient acetaldehyde adsorption/desorption.

2.2 Adsorption/desorption kinetics

From previous studies it is known that acetaldehyde effectively adsorbs on the TiO_2 surface [24,25]. Assuming monolayer coverage, equivalent adsorption sites, uniform surface and no adsorbate-adsorbate interaction – i.e. Langmuir behavior – then the rate of acetaldehyde adsorption, r_{ads} [mol m^{-2} s^{-1}] is given by (Eq.1).

$$r_{ads} = k_{ads} C_{Acal,bulk} (1 - \theta_{Acal}) \quad \text{(Eq.1)}$$

with k_{ads} [m s^{-1}] the adsorption rate constant, $C_{Acal,bulk}$ [mol m^{-3}] the bulk acetaldehyde concentration in the gas flow and θ_{Acal} the fractional coverage of acetaldehyde on active sites, which is in turn equivalent to the ratio of the acetaldehyde concentration adsorbed on the filter, $C_{Acal,filter}$ [mol kg^{-1}] over the total surface concentration of active sites provided by the filter, Γ_{filter} [mol kg^{-1}]. Note that the weight-based units of $C_{Acal,filter}$ and Γ_{filter} indicate that the VOC coverage is defined per unit of mass of the entire filter material, i.e. fiber mat support *plus* photocatalyst coating. This is a convenient definition since the applied amount of coating is so small that it cannot simply be measured by weighing. The rate of acetaldehyde desorption, r_{des} [mol m^{-2} s^{-1}] is given by (Eq.2).

$$r_{des} = k_{des} \theta_{Acal} \quad \text{(Eq.2)}$$

with k_{des} [mol m^{-2} s^{-1}] the desorption rate constant. At equilibrium, the rates of adsorption and desorption are equal and combination of (Eq.1) and (Eq.2) yields the well-known Langmuir-type expression (Eq.3), describing the variation of θ_{Acal} with the bulk acetaldehyde concentration:

$$\theta_{Acal} = \frac{K C_{Acal,bulk}}{1 + K C_{Acal,bulk}} = \frac{C_{Acal,filter}}{\Gamma_{filter}} \quad \text{(Eq.3)}$$

ACCEPTED MANUSCRIPT

with K [m^3 mol^{-1}] the Langmuir adsorption constant, given by the ratio of k_{ads} over k_{des}.

The adsorption parameters Γ_{filter} and K can be obtained for continuous flow systems by performing a simple adsorption test in which different bulk acetaldehyde concentrations are dosed to the reactor containing the filter at a fixed total flow rate, and determining the corresponding amount of pollutant adsorbed for each inlet concentration, at equilibrium conditions. The latter is possible due to the on-line FTIR monitoring of the acetaldehyde level at the outlet of our reactor. Linearization of (Eq.3) yields $(K\,\Gamma_{filter})^{-1}$ as the slope and Γ_{filter}^{-1} as the intercept in a plot of $C_{Acal,filter}^{-1}$ *versus* $C_{Acal,bulk}^{-1}$, as can be derived from (Eq.4).

$$\frac{1}{C_{Acal,filter}} = \frac{1}{K\Gamma_{filter}}\frac{1}{C_{Acal,bulk}} + \frac{1}{\Gamma_{filter}} \qquad \text{(Eq.4)}$$

Accurate determination of these adsorption parameters requires a geometrical correction that accounts for dead space in the reactor and the FTIR detection cell of the set-up, as this induces a time lapse in the signal registration that is not attributable to adsorption. In addition, adsorption is not completed instantaneously as the continuous gas flow is introduced to and crosses the reactor, but transient behavior is observed until the adsorption/desorption equilibrium is reached. Therefore, equilibrium values for $C_{Acal,filter}$ can only be obtained by integrating the transient, FTIR-measured acetaldehyde bulk concentrations at the reactor outlet over the period in which the rate of acetaldehyde adsorption is greater than the rate of desorption (i.e., until equilibrium is reached) (Eq.5):

$$C_{Acal,filter} = \frac{1}{\rho V}\int_{trans.\ period} \left(C_{Acal,bulk,eq} - C_{Acal,bulk}\right) Q\,dt \qquad \text{(Eq.5)}$$

where ρ [kg m^{-3}] and V [m^3] are the bulk density and volume of the filter, Q [m^3 s^{-1}] is the air flow rate through the reactor and $C_{Acal,bulk,eq}$ is the bulk acetaldehyde concentration at equilibrium. The correction for dead space in the reactor is done by performing tests with uncoated filters at the same fixed flow rate and the same bulk acetaldehyde concentrations as the adsorption tests. The values for $C_{Acal,filter}$, obtained from Eq.5 for these 'correction tests' were subtracted from the values obtained from the corresponding adsorption tests to account for the reactor dead space.

Whereas the aforementioned procedure to obtain the adsorption parameters requires several adsorption tests at different bulk acetaldehyde concentrations, as well as 'correction tests' using uncoated filters, CFD provides a useful tool to take all transient effects into account and therefore enables precise determination of the parameters under these conditions, as we will demonstrate below.

ACCEPTED MANUSCRIPT

2.3 Computational Fluid Dynamics approach

Air flow modeling

All theoretical simulations were performed using the commercial software package Comsol Multiphysics v.4.4. The CFD geometry of the photocatalytic test reactor including the FTIR detection cell and an impression of the computational grid are shown in Figure 1b. In the actual setup, the tube connecting the test reactor with the FTIR detection cell contained a few elbow bends and its length was over 50 cm, but considering the small tube diameter (4 mm) this corresponds to a negligible air volume as compared to the volume of both the reactor and the FTIR detection cell. For simplification and to reduce computation time this tube was replaced by a short straight tube section in the CFD geometry. For the same reasons and considering the symmetry of the geometry, only half of the geometry was meshed as shown in Figure 1b. The computational grid consisted of approximately 80,000 tetrahedral cells with refinement at the boundaries, inlet and outlet of the reactor. Grid size independency was ensured by gradually refining the mesh until further refinement did not affect the results. In this case, the average mesh quality of the geometry was 0.7571.

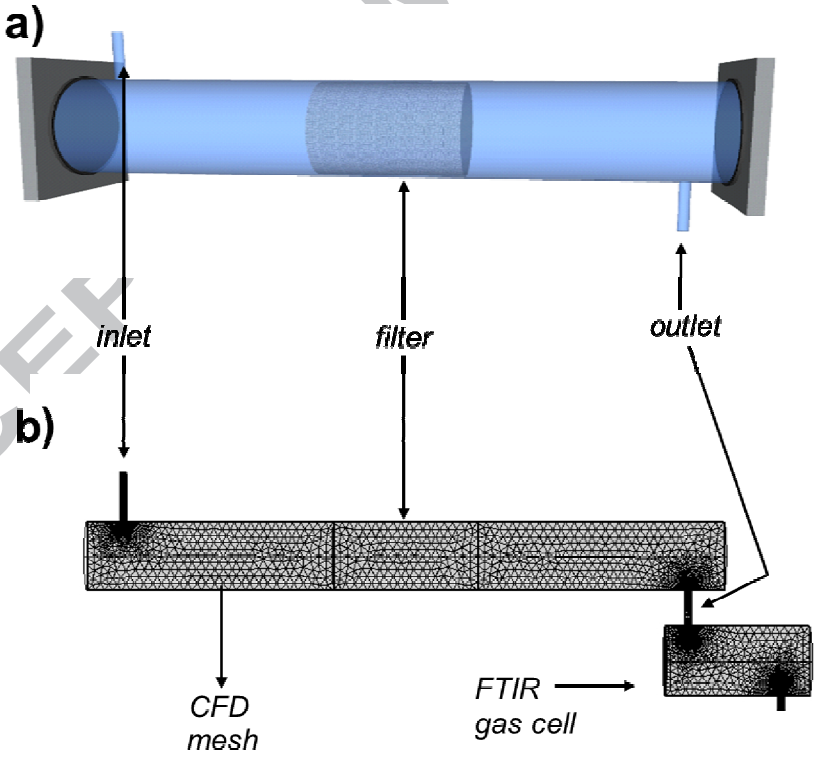

Figure 1. a) Schematic drawing (to scale) of the test reactor. b) representation of the reactor and FTIR gas cell geometry and mesh used in the CFD simulations. (color version online)

ACCEPTED MANUSCRIPT

Under the low flow rate conditions (400 cm^3 min^{-1}) used in this study, local Reynolds numbers are low, typically ranging from about 5 to 10 in the bulk of the reactor to about 800 in the small tubes connecting the different devices. This indicates that the reactor is operated in a laminar flow regime at all times and a laminar flow model can be used. The low velocities also permitted to model air as an incompressible fluid. All standard air properties are available in Comsol and were used as such in the simulations.

Whereas modeling laminar air flow in the bulk of the reactor is straightforward, the presence of the (coated or uncoated) glass fiber in the geometry requires some attention. A number of approaches are possible for describing flow in multiphase systems. In this work, the air velocity and pressure fields in the coated glass fiber were modeled using the Darcy-Forchheimer equation, which considers single-phase flow in a porous medium [26]. As compared to other approaches such as multiphase Eulerian models, Darcy's law is a convenient and computationally profitable approximation. As in Darcy's law, Darcy-Forchheimer states that the velocity field through a porous medium is determined by the pressure gradient $\Delta P/\Delta x$ [Pa m^{-1}], the fluid dynamic viscosity μ [Pa s], and the structure of the porous medium. In addition, it extends Darcy's law to include a term that accounts for the viscous transport in the momentum balance (Eq.6):

$$\frac{\Delta P}{\Delta x} = -\frac{\mu}{\kappa A} Q - \frac{\rho}{\kappa_1 A^2} Q^2 \qquad \text{(Eq.6)}$$

where κ [m^2] is the permeability of the porous medium, ρ [kg m^{-3}] its density and κ_1 [m] is the inertial permeability. A [m^2] is the cross-section of the filter perpendicular to the flow and Q [m^3 s^{-1}] is the volumetric flow rate. The term ρ/κ_1 is sometimes called the Forchheimer drag coefficient. For the glass fiber mats, the permeability was measured from pressure drop experiments using an anemometer (Kimo CTV 110, Kimo Instruments, France) and a differential pressure sensor (Fluke 717 30G, Fluke Corporation, US). The Darcy-Forchheimer equation was coupled with the laminar flow calculations by using the pressure at the boundary of the fluid and the fiber filter as a boundary condition in the Darcy-Forchheimer module.

Using the appropriate air flow rate (400 cm^3 min^{-1}) at the reactor inlet and the fiber filter properties determined from pressure drop experiments, a steady-state solution for the air flow in the reactor was generated using a direct, stationary solver (relative tolerance 0.001). Second order discretization was set by default in all equations. In the subsequent transient CFD analysis where advection, diffusion and adsorption/desorption of acetaldehyde was studied, this stationary solution was considered to describe the air flow during the entire second phase of each adsorption test (the 45 min required to achieve adsorption-desorption

ACCEPTED MANUSCRIPT

equilibrium). This approach was a last simplification in the analysis and greatly reduced the computational requirements. In reality, short-lived transient phenomena occur each time the setup switches from by-pass to reactor modus. Modeling these phenomena requires the coupled solution of both time dependent air flow and species transport. In an analysis where parameters are to be optimized (see further), such approach would lead to extremely lengthy calculations which do not justify the rather confined improvement in the approximation of reality.

Transport of acetaldehyde

The steady-state air flow solution was coupled with the scalar transport equation to account for time-dependent advection and diffusion of acetaldehyde during the second phase of the adsorption test. A time-dependent solver with relative tolerance 0.0001 as convergence criterion was used. In the flow regions where no filter was present, transport of acetaldehyde was calculated as (Eq.7):

$$\frac{\partial C_{Acal,bulk}}{\partial t} = \nabla \cdot \left(D \nabla C_{Acal,bulk} \right) - \mathbf{u} \cdot \nabla C_{Acal,bulk} \qquad \text{(Eq.7)}$$

with **u** being the (stationary but spatially varying) velocity vector of the air [m s^{-1}], and D the mass diffusion coefficient of acetaldehyde in air [m^2 s^{-1}]. The mass diffusion coefficient for acetaldehyde in air was taken as 11.5×10^{-6} m^2 s^{-1} [27]. In Eq.7, the first term on the right-hand side describes the change in acetaldehyde concentration due to diffusion which is proportional to the Laplacian or second derivative of concentration. The second right-hand side term describes convection or advection of acetaldehyde (or the change in concentration as a result of flow).

To include adsorption/desorption, a second species $C_{Acal,filter}$ was defined to differentiate between acetaldehyde in the bulk gas phase $C_{Acal,bulk}$ and its adsorbed counterpart on the filter material. In the flow region of the filter, adsorption and desorption of acetaldehyde were included as reaction rate expressions in the $C_{Acal,bulk}$ transport equation (Eq.8):

$$\frac{\partial C_{Acal,bulk}}{\partial t} = \nabla \cdot \left(D \nabla C_{Acal,bulk} \right) - \mathbf{u} \cdot \nabla C_{Acal,bulk} - r_{ads} + r_{des} \qquad \text{(Eq.8)}$$

where the reaction rates for adsorption and desorption are given by Eqs.1 and 2. Notice that adsorption was considered as a sink term and desorption as a source of $C_{Acal,bulk}$. Accordingly, for the new species $C_{Acal,filter}$ an analogous transport equation with the same reaction rate

ACCEPTED MANUSCRIPT

expressions was used but here adsorption is a source term with positive sign and desorption was a sink term with negative sign. In this way, conservation of mass was ensured.

The acetaldehyde transport equations were used to model advection, diffusion, adsorption and desorption during the second phase of the adsorption tests. For each particular test, the initial conditions were defined as $C_{Acal,bulk} = C_{Acal,filter} = 0$ in the reactor and $C_{Acal,bulk} = C_{Acal,test}$, i.e. the experimentally verified steady-state bulk concentration of the contaminated gas flow measured by FTIR in by-pass mode. Then the stationary air flow solution was coupled with the transient scalar transport equations to model advection, diffusion, adsorption and desorption. Hereby the appropriate acetaldehyde concentration was used as a boundary condition at the reactor inlet.

Parameter estimation

For determining the parameters k_{ads}, k_{des} and Γ_{filter}, a Comsol optimization module was used in conjunction with the CFD calculations. Parameter estimation involves correlating the model to experimental data. In our experiments, where concentrations change as a function of time a least squares objective function was defined as (Eq.9):

$$Obj = \sum_{t} \left(C_{Acal,out,exp,t} - C_{Acal,out,CFD,t} \right)^2 \qquad \text{(Eq.9)}$$

where $C_{Acal,out,exp,t}$ and $C_{Acal,out,,CFD,t}$ are the experimental and predicted outlet concentrations at a particular time t, respectively. The SNOPT (Sparse Nonlinear OPTimizer) algorithm developed by Gill *et al.* was used for finding the local minimum of the objective function by changing the kinetic parameters within certain constraints [28]. For the predicted outlet concentration $C_{Acal,out,,CFD,t}$, the volume-averaged acetaldehyde concentration in the FTIR cell, as calculated using the CFD model, was calculated at each time step. Since the FTIR spectrometer uses the complete volume of the FTIR cell for measuring the absorption spectrum, the value for outlet concentration obtained after volume averaging corresponds best with the experimental result. CFD calculated volume-averaged acetaldehyde concentrations in the FTIR cell were therefore used and compared to the experimentally obtained $C_{Acal,out,exp}$ in all cases. By doing this at each time step and summing the resulting squared differences in the objective function, intrinsic adsorption parameters can be estimated that are valid for the whole range of prevailing concentrations. Considering the Langmuir model, the rates for adsorption and desorption are coupled through the adsorption constant K. Therefore, one of the rate constants can be fixed. In our work, k_{des} was fixed at a unity value leaving only k_{ads} and Γ_{filter} as unknown parameters to be estimated.

ACCEPTED MANUSCRIPT

3. Results and Discussion

3.1. Acetaldehyde adsorption/desorption: analytic approach

Figure 2 shows the acetaldehyde concentration over time during the two phases of the measurement, corresponding to flow directly to the detector (i.e. by-pass, 0 – 10 min) and flow through the reactor containing the filter under dark conditions (after minute 10). Figure 2a shows acetaldehyde concentrations for experiments where non-coated fiber filters were used, whereas Figure 2b shows results for sample A. In both cases, acetaldehyde concentrations ranged roughly between 0,0002 and 0,0035 mol/m^3. For the other sample, analogous concentration profiles were obtained. The steep drop in the acetaldehyde level at minute 10 and the subsequent transient behavior until the steady state level is re-established, can be attributed to three phenomena: (1) displacement of the dead air in the reactor and FTIR detection cell volumes by the polluted gas flow, (2) time delay caused by retardation of acetaldehyde molecules in the fiber network and (3) adsorption on the photocatalytic filter. Only the latter yields useful parameters for describing the filter system (Γ_{filter}), however, the other effects need to be taken into account as well for accurate analysis.

ACCEPTED MANUSCRIPT

ACCEPTED MANUSCRIPT

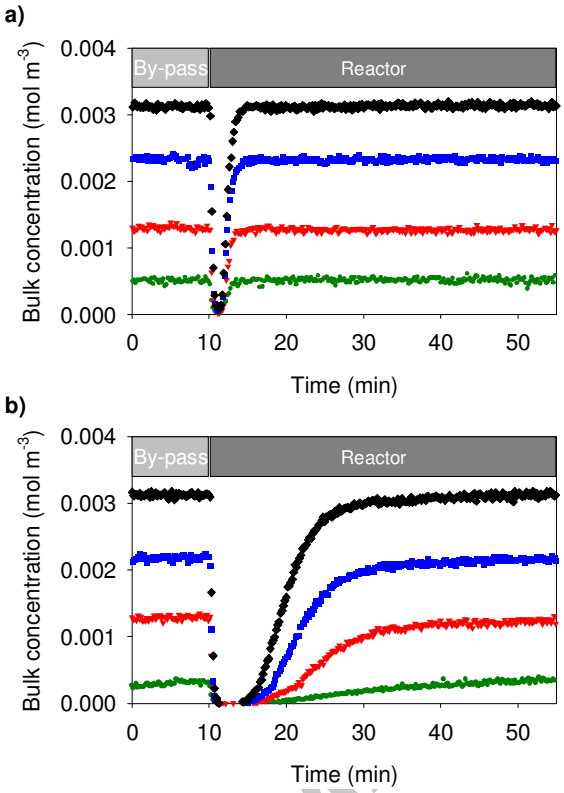

Figure 2. Measured bulk concentration profiles of acetaldehyde when switching from by-pass to the filter reactor with a) uncoated fibers and b) coated fibers (sample A) for four different inlet concentrations at 400 cm^3 min^{-1} total flow rate. (color version online)

The air displacement effect and retardation of acetaldehyde molecules were accounted for by analysis of the experiments with uncoated filters (Figure 2a). Experiments with empty reactors (no fiber filter present) were also performed and revealed that the presence of the filter did not significantly change the obtained concentration profiles (see further, Figure 5). This indicates that retardation of acetaldehyde molecules in the fiber network is negligible and that no significant adsorption occurs on the uncoated fibers. Equilibrium values for $C_{Acal,filter}$ were obtained by integration over the transient period (Eq.5) and correction for dead space in the reactor. The results for each of the samples are shown in Figure 3. In this figure, the full lines represent Langmuir isotherms using the adsorption parameters Γ_{filter} and K that were derived from the slope and intercept of a plot of $C_{Acal,filter}^{-1}$ *versus* $C_{Acal,bulk}^{-1}$ for each individual sample, as given by Eq.4. The values obtained for the adsorption parameters are given in Table 1. Using a colloidal suspension at higher TiO_2 concentration (sample B) clearly enhances the amount of catalyst bound on the fibers, as demonstrated by the higher value for Γ_{filter}. Since there is no particular reason why the Langmuir adsorption constant should depend on the amount of catalyst bound, Langmuir isotherms were also derived from regression using

ACCEPTED MANUSCRIPT

an optimization solver, whereby the same Langmuir adsorption coefficient was considered for each of the two cases. The results of this regression are included in Figure 3 (red dotted lines) and the corresponding parameters are given in Table 1. A constant adsorption coefficient seems a more logical deduction from the Langmuir model and the latter parameters were used in further analysis.

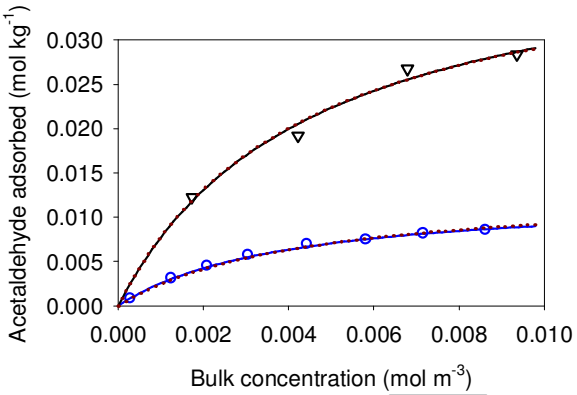

Figure 3. Adsorbed acetaldehyde concentration on the filter material, $C_{Acal,filter}$ (mol kg^{-1}) *versus* the bulk acetaldehyde concentration, $C_{Acal,bulk}$ (mol m^{-3}) for sample A (blue ○) and sample B (black ▽), fitted by a Langmuir-type adsorption isotherm using the analytically obtained parameters from the individual regressions in Table 1 (solid lines), and the regression based on a unique value for *K* for both data sets (red dotted lines). (color version online)

Table 1. Langmuir regression parameters from analytical solution

	Parameters from individual regression		Parameters from regression with unique K value	
	Γ_{filter} (mol kg^{-1})	K (m^3 mol^{-1})	Γ_{filter} (mol kg^{-1})	K (m^3 mol^{-1})
Sample A	0.0126	255	0.0133	228
Sample B	0.0425	222	0.0420	228

3.2. Acetaldehyde adsorption/desorption: CFD approach

Before using the CFD model, the Darcy-Forchheimer parameters were derived from measurements of the pressure drop as a function of the flow velocity through the filter medium. Results for these measurements are shown in Figure 4. From the results, the permeability and the Forchheimer drag coefficient were derived using regression (solid line in Figure 4). For the fiber filters used in this work, permeability was 3.8×10^{-7} m^2 and the Forchheimer drag coefficient was 29 kg·m^{-4}. When using the Darcy-Forchheimer law in the governing CFD equations, the porosity of the medium is also required. Porosity is a

ACCEPTED MANUSCRIPT

dimensionless property defined as the fraction of the volume that is occupied by pores, and was theoretically calculated from the bulk volume and the measured weight of the glass fiber filter. For this medium, porosities higher than 99% were obtained.

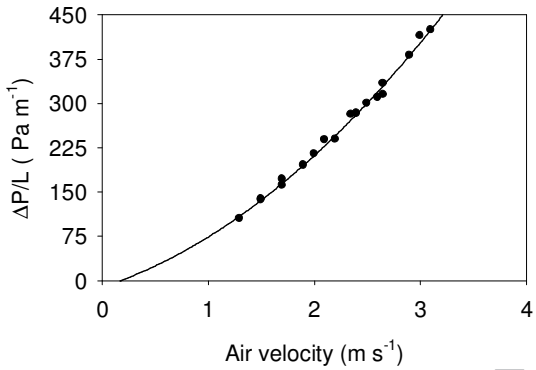

Figure 4. Pressure drop per unit length as a function of air velocity (data points) with a regression analysis based on the Darcy-Forchheimer equation (solid line) in order to determine the filter permeability and Forchheimer drag coefficient.

Whereas experiments with uncoated filters or with empty reactors were needed to correct for reactor dead space in the analytic approach, such comparative simulations were not needed in the CFD approach since the transient phenomena are implicitly accounted for. In order to verify the validity of this implicit air displacement correction by CFD, simulations were performed for the reference cases of an empty reactor and a reactor filled with uncoated filter material. Typical CFD results (volume-averaged acetaldehyde concentration in the FTIR cell) for tests at different acetaldehyde concentrations are shown in Figure 5, and (stationary) velocity profiles are shown in Figure 6. For the tests with uncoated filter (Figure 5a) the Darcy-Forchheimer approach was included in the calculations but no adsorption/desorption. For the empty reactor (Figure 5b), no porous medium was included. The experimental agreement with the CFD simulations was sufficiently convincing to reliably proceed with the methodology, as evidenced by the overall coefficients of determination equaling 0.959 and 0.973 for Figures 5a and b respectively. The agreement also indicates the validity of the velocities and flow rate calculated by the CFD model. Again, notice that the presence of the filter exerts no significant influence on acetaldehyde transport in the reactor. This is not surprising considering the low density, high porosity and permeability of the filter. Furthermore, no significant acetaldehyde adsorption occurs on uncoated fibers as indicated by the almost perfect conformity of Figure 5a and b. Hence, the drop in the acetaldehyde level in Figure 5a and b is only due to dead air displacement and this is accounted for by the model. Any additional drop in the acetaldehyde level in (Figure 2b as compared to Figure 2a) is

ACCEPTED MANUSCRIPT

attributed to adsorption on the coated fibers. As an additional test, the validity of the CFD model was also explored at a higher air flow rate (1200 *vs.* 400 $cm^3 min^{-1}$) and a typical result – with promising agreement– is shown in Figure 5c ($R^2 = 0.958$).

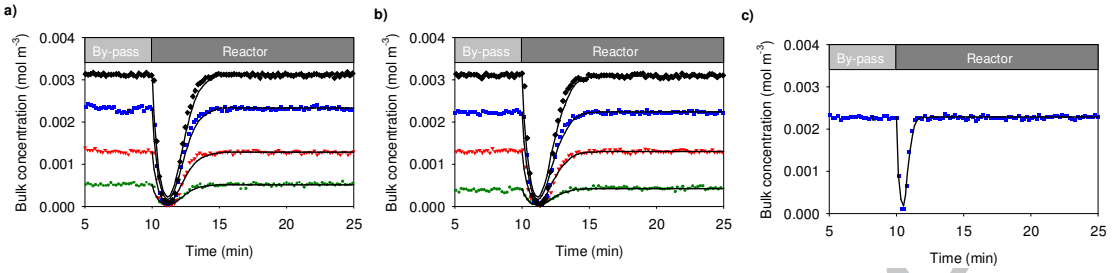

Figure 5. CFD simulation results (solid black lines) for several reference cases at different bulk acetaldehyde inlet concentrations (colored data points): a) reactor with uncoated filter material, b) empty reactor and c) empty reactor at a higher total gas flow rate (1200 cm^3 min^{-1} instead of 400 cm^3 min^{-1}). (color version online)

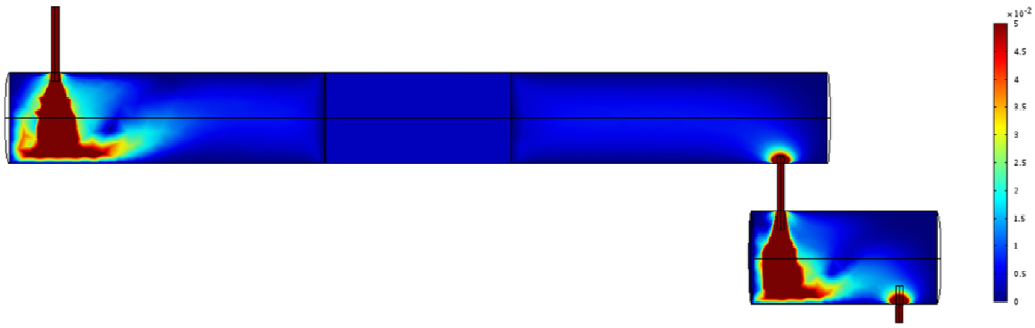

Figure 6. CFD velocity profile (m s^{-1}) for the reactor with filter material (inlet flow rate 400 cm^3 min^{-1}). (color version online)

One of the main advantages of CFD is that both the acetaldehyde bulk and surface concentrations can be calculated at any given time, at any given location in the system throughout the entire adsorption process. This clearly exposes the limits of the analytical solution, which can only account for steady state situations. In contrast, CFD also accurately accounts for the entire transient regime prior to achieving stationary levels. An illustration of how the acetaldehyde bulk and surface concentrations can be simulated by CFD is given in Figure . A drastic change in the acetaldehyde concentration (both in the bulk as well as on the surface) can be clearly observed as one moves along the filter, due to adsorption. An animation of the entire transient adsorption process, modeled by CFD is available as a Supplementary Information movie. At first the displacement of still-standing air in the reactor and FTIR gas cell is observed, after which acetaldehyde passes the reactor as a plug flow. The acetaldehyde concentration is attenuated at the location of the filter. As the surface concentration on the filter increases, visualized as the rectangle above the reactor at the

ACCEPTED MANUSCRIPT

location of the filter material becoming more and more black, the high inlet acetaldehyde concentration finally breaks through until a steady state concentration is reached throughout the entire system.

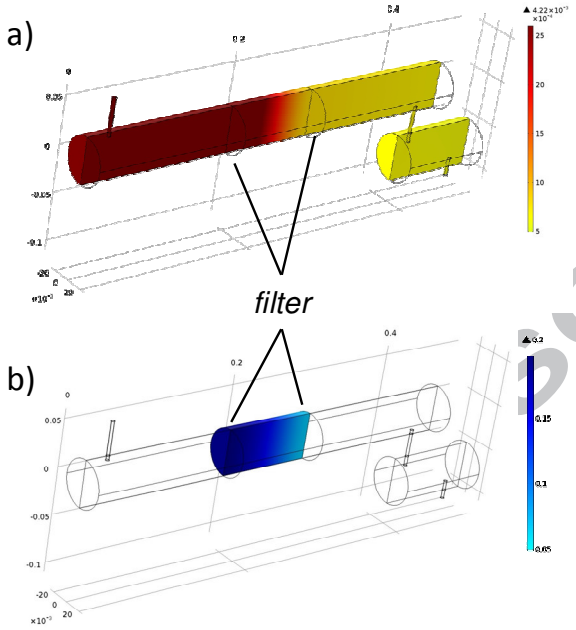

Figure 7. Variation of the acetaldehyde concentration a) in the bulk and b) adsorbed on the filter as modeled by CFD at minute 17 in the measurement cycle for sample B at an inlet concentration of 0.004 mol m^{-3} and total gas flow rate of 400 cm^3 min^{-1}. (color version online)

Using the optimization routine, the adsorption/desorption parameters were estimated for each of the samples. Instead of using the optimization routine separately for each independent experiment, parameter estimation was done simultaneously using all experiments performed for a sample (i.e., for each particular sample A or B, the objective function was evaluated for the complete set of experiments at different acetaldehyde inlet concentrations). In fact, CFD could be applied to estimate the adsorption parameters even from one single experiment (i.e. one single concentration for one sample). Evidently, this would result in lower accuracy of the values obtained, as it is heavily subjected to experimental fluctuations in that case. As an initial guess for the parameters, the analytically obtained values (given in the last two columns of Table1) were used. The results for the optimization are shown in Figure . The resulting optimized values for k_{ads} and Γ_{filter} enabled to numerically replicate the experimentally determined outlet concentrations with deviations smaller than 2%. The values for the optimized parameters are listed in Table 2. From the table it can be seen that the

ACCEPTED MANUSCRIPT

optimized adsorption parameters show the same trends as the ones obtained using the analytic approach (first two columns in Table 1).

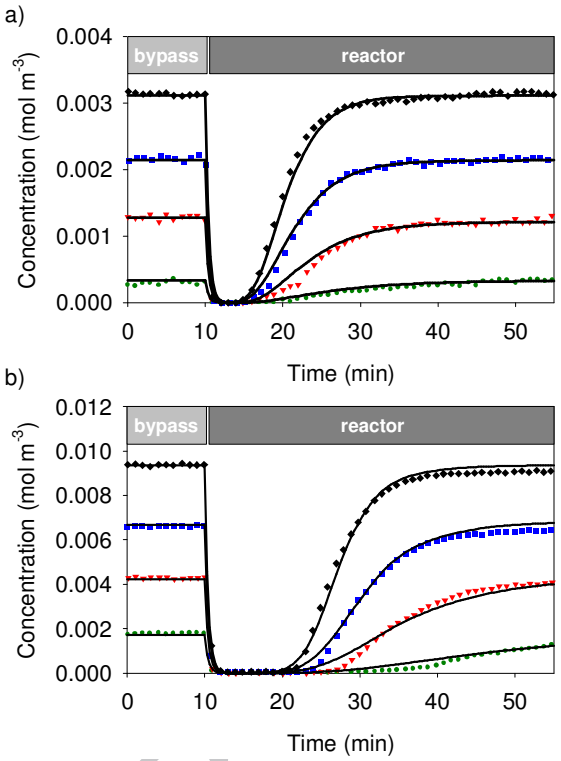

Figure 8. CFD simulations (solid black lines) based on optimized adsorption parameters of the adsorption experiments at different acetaldehyde inlet concentrations (colored data points) for a) sample A and b) sample B. Notice that in the latter case the CFD simulations overestimate the actual acetaldehyde levels for the highest inlet concentrations. (color version online)

3.3. Fine-tuning of the model: Aldol condensation

When comparing the CFD concentration profiles with experimental ones, in some cases a slight overestimation of the acetaldehyde outlet concentration was observed when the equilibrium was reached. More specifically, this was observed for sample B (with the highest amount of catalyst) when the bulk acetaldehyde concentration was in the higher range, as can be seen after 40 min in Figure b at concentrations exceeding 0.006 mol/m^3. The equilibrium concentration was only gradually reached whereas the CFD model did not show this behavior. When acetaldehyde is adsorbed on TiO_2, it can undergo an aldol condensation to crotonaldehyde [29–32]. This was also observed in an in situ FTIR study by Hauchecorne *et al.* [25]. A way to deal with the aldol condensation is by introducing the following rate expression (Eq.10),

ACCEPTED MANUSCRIPT

$$r_{aldol} = k_{aldol}(C_{Acal,filter})^2 \quad \text{(Eq.10)}$$

since two acetaldehyde molecules are involved in the reaction. From the literature, there is evidence that crotonaldehyde is bound to two active sites on the catalyst, whereas acetaldehyde occupies one site. The molecular formation mechanism is schematically represented in the work by Singh *et al.* [31]. Furthermore, crotonaldehyde is more strongly bound to the catalyst. If we therefore assume that crotonaldehyde irreversibly binds to the catalyst (i.e., negligible desorption of crotonaldehyde as compared to mono-molecular acetaldehyde), then the rates of acetaldehyde adsorption and desorption become (Eq.11):

$$r_{ads} = k_{ads}C_{Acal,bulk}(1 - \theta_{Acal} - \theta_{Crot})$$
$$r_{des} = k_{des}\theta_{Acal} \quad \text{(Eq.11)}$$

where θ_{Crot} represents the fractional coverage of crotonaldehyde on active sites. Notice that during the course of the adsorption/desorption phase, the rates of both adsorption and desorption gradually decrease since a fraction θ_{Crot} of the available sites are gradually occupied by the more strongly bound crotonaldehyde. In case an aldol condensation occurs, no exact adsorption/desorption equilibrium is reached as in ordinary Langmuir adsorption since one of the main boundary conditions of the model is violated; i.e. adsorbate-adsorbate interaction do occur in this case. Furthermore, this also implies that analytical determination of the adsorption parameters becomes difficult due to the additional unknown parameter k_{aldol} (that governs θ_{Crot}) and linearization of the adsorption equation (as in eq. 4) is no longer possible to extract all relevant parameters simultaneously. Including the reactions in a CFD model on the other hand can be an interesting approach to study what the effects of aldol condensation are on the progress of adsorption/desorption. We have employed CFD to derive all information required to describe the adsorptive properties of the photocatalytic filter material. This way the acetaldehyde levels can be accurately modeled, even in the transient zones of the process where analytical solutions would otherwise fail.

The optimized results are shown in Figure and the corresponding parameters are included in

Table 2. Despite the fact that the adsorption parameters did not change significantly, a far better agreement was observed for the formerly mentioned cases. This is also apparent from the generally improved coefficients of determination for the agreement between

ACCEPTED MANUSCRIPT

simulation and experiment for the cases in Figure 8 (aldol condensation not included) versus Figure 9 (aldol condensation included) (Table 3). Apparently the fact that the acetaldehyde concentration is more gradually reached can be ascribed to the formation of an intermediate or a byproduct (crotonaldehyde) which is more strongly bound to the catalyst surface. The CFD optimization routine yields an average value for k_{aldol} of (3.3 ± 0.6) $\times 10^{-4}$ m^3 mol^{-1} s^{-1} for all experiments at different acetaldehyde concentrations for samples A and B. The analytic approach considering Langmuir behavior alone does not account for this phenomenon.

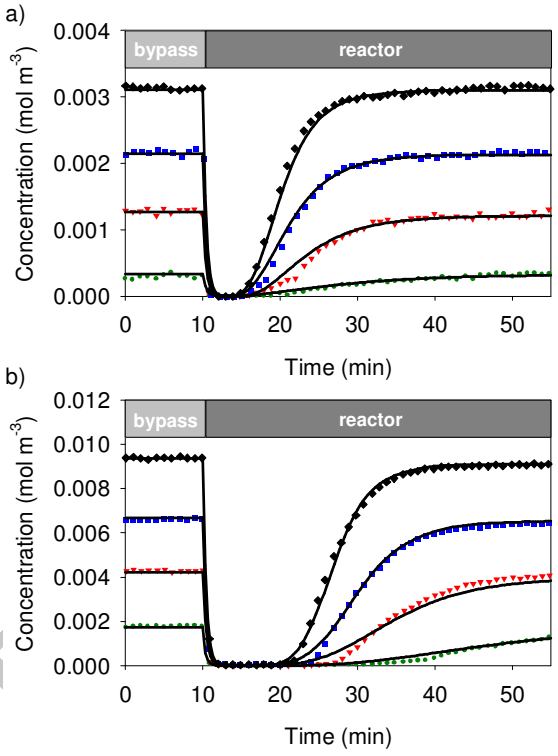

Figure 9. CFD simulations (solid black lines) based on optimized adsorption parameters of the adsorption experiments at different acetaldehyde inlet concentrations (colored data points) for a) sample A and b) sample B by taking into account the irreversible aldol condensation reaction on the catalyst surface. (color version online)

Table 2. Estimation of the adsorption parameters using CFD with an optimization routine based on the simple Langmuir model and the extended model that accounts for aldol condensation on the surface.

	Parameters from CFD optimization		Parameters from CFD optimization including aldol condensation on the surface	
	Γ_{filter} (mol kg^{-1})	K (m^3 mol^{-1})	Γ_{filter} (mol kg^{-1})	K (m^3 mol^{-1})
Sample A	0.0120	222	0.0119	220
Sample B	0.0410	198	0.0382	221

ACCEPTED MANUSCRIPT

Table 3. Coefficients of determination (R^2) for the various CFD simulations indicating the 'goodness of fit' of the CFD models.

	Concentration			
	1 (lowest)	2	3	4 (highest)
Fig 8a	0.8891	0.9813	0.9959	0.9956
Fig 8b	0.9206	0.9876	0.9933	0.9964
Fig 9a	0.9362	0.9845	0.9951	0.9965
Fig 9b	0.9497	0.9839	0.9972	0.9987

In a final validation experiment, the obtained optimized adsorption parameters (with inclusion of aldol condensation) were used to simulate the (transient) adsorption behavior of acetaldehyde at a different, higher flow rate, i.e. 1200 mL min^{-1} instead of 400 mL min^{-1} as in all previous adsorption experiments. The CFD simulation result for two different inlet concentrations is given by the solid lines in Figure 10. The simulations were experimentally verified, represented as data points in Figure 10. From this validation experiment we conclude that the intrinsic adsorption parameters given in Table 2 are quite reliable, as evidenced by the coefficients of determination amounting to 0.960 and 0.970 for the high and low acetaldehyde inlet levels respectively.

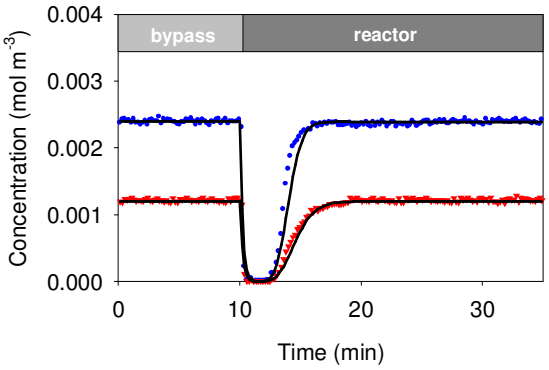

Figure 10. CFD simulations (solid black lines) of acetaldehyde adsorption behavior on sample A based on the optimized adsorption parameters accounting for aldol condensation for two different inlet concentrations at a total flow rate of 1200 mL min^{-1}. Experimental verification is represented as colored data points. (color version online)

Conclusions

CFD proved to be a versatile and accurate tool to extract all relevant acetaldehyde adsorption parameters, even for situations in which analytical estimations would otherwise fail. In addition to steady-state values, CFD also provided time- and location-dependent adsorption data, both in the bulk and on the surface. It enabled an implicit correction for air displacement effects in the reactor and detection gas cell. The CFD method also facilitated the

ACCEPTED MANUSCRIPT

extension of the traditional Langmuir behavior by adding an irreversible surface aldol condensation reaction to the model. After applying an optimization routine, the CFD simulations yielded an adsorption constant of 220 m^3 mol^{-1} in addition to the maximum adsorption capacity (Γ_{filter}) values of both filter materials tested. These parameters can be considered as highly accurate input variables for further photocatalytic kinetic analysis and thus the future development of air purifiers based on photocatalytic filters integrated in continuous flow systems.

Acknowledgement

S.W.V. acknowledges the Research Foundation – Flanders (FWO) for a postdoctoral fellowship. M.K. acknowledges the IWT for a PhD fellowship. Konstantina Kalafata and Ioanna Fasaki are greatly thanked for providing the NanoPhos suspension. Bioscience Engineering bachelor students M. Gerritsma, J. Helsen and Y. Riahi Drif are thanked for their assistance in performing the adsorption experiments.

References

[1] J. Mo, Y. Zhang, Q. Xu, J.J. Lamson, R. Zhao, Photocatalytic purification of volatile organic compounds in indoor air: A literature review, Atmos. Environ. 43 (2009) 2229–2246.

[2] Y. Paz, Application of TiO_2 photocatalysis for air treatment: Patents' overview, Appl. Catal. B-Environmental. 99 (2010) 448–460.

[3] J. Zhao, X. Yang, Photocatalytic oxidation for indoor air purification: a literature review, Build. Environ. 38 (2003) 645–654.

[4] S. Pigeot-Remy, J.C. Lazzaroni, F. Simonet, P. Petinga, C. Vallet, P. Petit, et al., Survival of bioaerosols in HVAC system photocatalytic filters, Appl. Catal. B Environ. 144 (2014) 654–664.

[5] K.-P. Yu, G.W.-M. Lee, W.-M. Huang, C.-C. Wu, C. Lou, S. Yang, Effectiveness of photocatalytic filter for removing volatile organic compounds in the heating, ventilation, and air conditioning system., J. Air Waste Manag. Assoc. 56 (2006) 666–74.

[6] S.W. Verbruggen, TiO_2 photocatalysis for the degradation of pollutants in gas phase: From morphological design to plasmonic enhancement, J. Photochem. Photobiol. C Photochem. Rev. 24 (2015) 64–82.

[7] S.J. Klaine, P.J.J. Alvarez, G.E. Batley, T.F. Fernandes, R.D. Handy, D.Y. Lyon, et al., Nanomaterials in the environment: behavior, fate, bioavailability, and effects., Environ. Toxicol. Chem. 27 (2008) 1825-1851.

ACCEPTED MANUSCRIPT

[8] J. Zhang, W. Song, J. Guo, J. Zhang, Z. Sun, L. Li, et al., Cytotoxicity of different sized TiO2 nanoparticles in mouse macrophages., Toxicol. Ind. Health. 29 (2013) 523–33.

[9] M.M. Hossain, G.B. Raupp, S.O. Hay, T.N. Obee, Three-dimensional developing flow model for photocatalytic monolith reactors, Aiche J. 45 (1999) 1309–1321.

[10] M. Hossain, G. Raupp, Polychromatic radiation field model for a honeycomb monolith photocatalylic reactor, Chem. Eng. Sci. 54 (1999) 3027–3034.

[11] M.L. Sauer, D.F. Ollis, Photocatalyzed oxidation of ethanol and acetaldehyde in humidified air, J. Catal. 158 (1996) 570–582.

[12] S.W. Verbruggen, S. Deng, M. Kurttepeli, D.J. Cott, P.M. Vereecken, S. Bals, et al., Photocatalytic acetaldehyde oxidation in air using spacious TiO_2 films prepared by atomic layer deposition on supported carbonaceous sacrificial templates, Appl. Catal. B Environ. 160-161 (2014) 204–210.

[13] M. Kurttepeli, S. Deng, S.W. Verbruggen, G. Guzzinati, D.J. Cott, S. Lenaerts, et al., Synthesis and characterization of photoreactive TiO_2–carbon nanosheet composites, J. Phys. Chem. C. 118 (2014) 21031–21037.

[14] S. Deng, S.W. Verbruggen, Z. He, D.J. Cott, P.M. Vereecken, J.A. Martens, et al., Atomic layer deposition-based synthesis of photoactive TiO_2 nanoparticle chains by using carbon nanotubes as sacrificial templates, RSC Adv. 4 (2014) 11648-11653.

[15] B. Sanchez, J.M. Coronado, R. Caudal, R. Portela, I. Tejedor, M.A. Anderson, et al., Preparation of TiO_2 coatings on PET monoliths for the photocatalytic elimination of trichloroethylene in the gas phase, Appl. Catal. B Environ. 66 (2006) 295–301.

[16] S.B. Kim, H.T. Hwang, S.C. Hong, Photocatalytic degradation of volatile organic compounds at the gas-solid interface of a TiO_2 photocatalyst, Chemosphere. 48 (2002) 437–444.

[17] L.L.P. Lim, R.J. Lynch, S.I. In, Comparison of simple and economical photocatalyst immobilisation procedures, Appl. Catal. A Gen. 365 (2009) 214–221.

[18] S.W. Verbruggen, S. Ribbens, T. Tytgat, B. Hauchecorne, M. Smits, V. Meynen, et al., The benefit of glass bead supports for efficient gas phase photocatalysis: Case study of a commercial and a synthesised photocatalyst, Chem. Eng. J. 174 (2011) 318–325.

[19] S. Brosillon, L. Lhomme, C. Vallet, A. Bouzaza, D. Wolbert, Gas phase photocatalysis and liquid phase photocatalysis: Interdependence and influence of substrate concentration and photon flow on degradation reaction kinetics, Appl. Catal. B Environ. 78 (2008) 232–241.

[20] I. Di Somma, L. Clarizia, S. Satyro, D. Spasiano, R. Marotta, R. Andreozzi, A kinetic study of the simultaneous removal of EDDS and cupric ions from acidic aqueous solutions by TiO_2-based photocatalysis under artificial solar light irradiation and deaerated batch conditions, Chem. Eng. J. 270 (2015) 519–527.

[21] R. Dillert, J. Stötzner, A. Engel, D.W. Bahnemann, Influence of inlet concentration and light intensity on the photocatalytic oxidation of nitrogen(II) oxide at the surface of Aeroxide® TiO_2 P25., J. Hazard. Mater. 211-212 (2012) 240–246.

ACCEPTED MANUSCRIPT

[22] A.S. Besov, A.V. Vorontsov, V.N. Parmon, Fast adsorptive and photocatalytic purification of air from acetone and dimethyl methylphosphonate by TiO_2 aerosol, Appl. Catal. B Environ. 89 (2009) 602–612.

[23] S.W. Verbruggen, S. Lenaerts, S. Denys, Analytic versus CFD approach for kinetic modeling of gas phase photocatalysis, Chem. Eng. J. 262 (2015) 1–8.

[24] S.W. Verbruggen, K. Masschaele, E. Moortgat, T.E. Korany, B. Hauchecorne, J.A. Martens, et al., Factors driving the activity of commercial titanium dioxide powders towards gas phase photocatalytic oxidation of acetaldehyde, Catal. Sci. Technol. 2 (2012) 2311–2318.

[25] B. Hauchecorne, D. Terrens, S. Verbruggen, J.A. Martens, H. Van Langenhove, K. Demeestere, et al., Elucidating the photocatalytic degradation pathway of acetaldehyde: An FTIR in situ study under atmospheric conditions, Appl. Catal. B Environ. 106 (2011) 630-638.

[26] A. Bejan, Convection heat transfer, John Wiley & Sons, Inc., Hoboken, NJ, USA, (2013).

[27] C.R. Sherwood, T. K., Pigford, R. L., and Wilke, Mass Transfer, McGraw-Hill, New York, (1975).

[28] P.E. Gill, W. Murray, M.A. Saunders, SNOPT: An SQP algorithm for large-scale constrained Optimization, SIAM J. Optim. 12 (2002) 979–1006.

[29] J. Raskó, J. Kiss, Adsorption and surface reactions of acetaldehyde on TiO_2, CeO_2 and Al_2O_3, Appl. Catal. A Gen. 287 (2005) 252–260.

[30] J.E. Rekoske, M.A. Barteau, Competition between acetaldehyde and crotonaldehyde during adsorption and reaction on anatase and rutile titanium dioxide, Langmuir. 15 (1999) 2061–2070.

[31] M. Singh, N. Zhou, D.K. Paul, K.J. Klabunde, IR spectral evidence of aldol condensation: Acetaldehyde adsorption over TiO_2 surface, J. Catal. 260 (2008) 371–379.

[32] H. Idriss, K.S. Kim, M.A. Barteau, Carbon-carbon bond formation via aldolization of acetaldehyde on single crystal and polycrystalline TiO_2 surfaces, J. Catal. 139 (1993) 119–133.

ACCEPTED MANUSCRIPT

1 **List of Figures in grayscale for printed version:**

2

3 **Figure 1 (print version)**

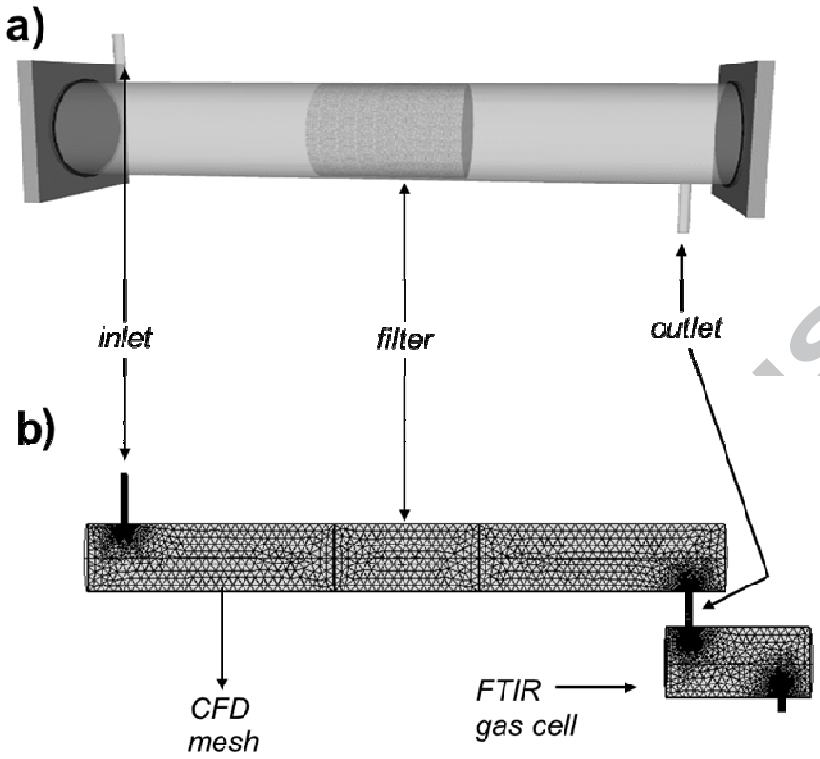

4

ACCEPTED MANUSCRIPT

ACCEPTED MANUSCRIPT

1 **Figure 2 (print version)**

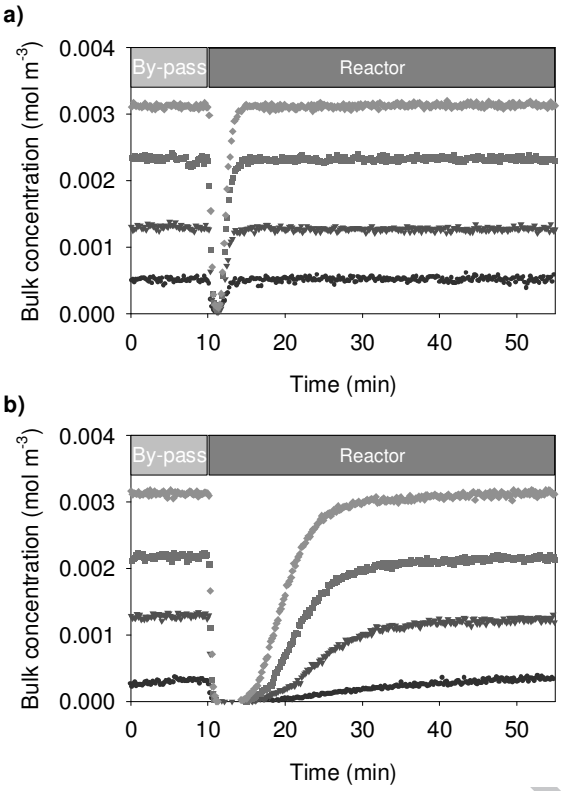

2

3

ACCEPTED MANUSCRIPT

ACCEPTED MANUSCRIPT

1 **Figure 3 (print version)**

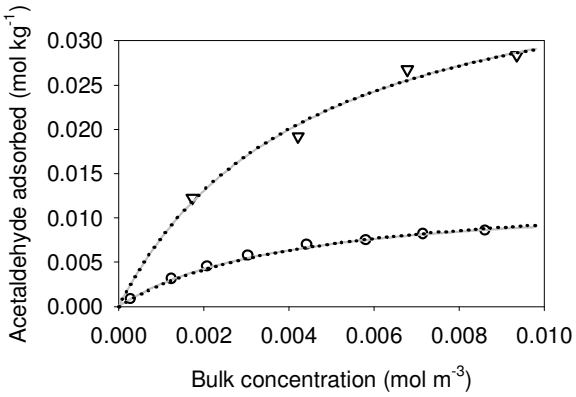

2

3

ACCEPTED MANUSCRIPT

ACCEPTED MANUSCRIPT

1 **Figure 4 (print version)**

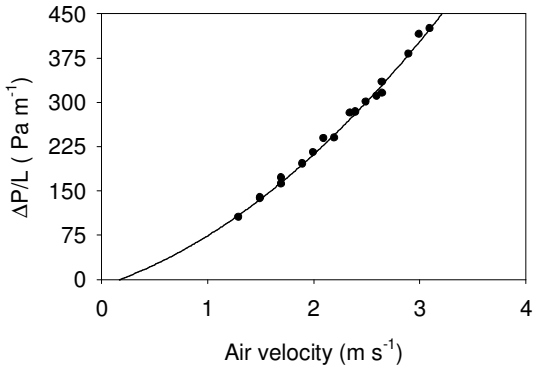

2

3

ACCEPTED MANUSCRIPT

ACCEPTED MANUSCRIPT

1 **Figure 5 (print version)**

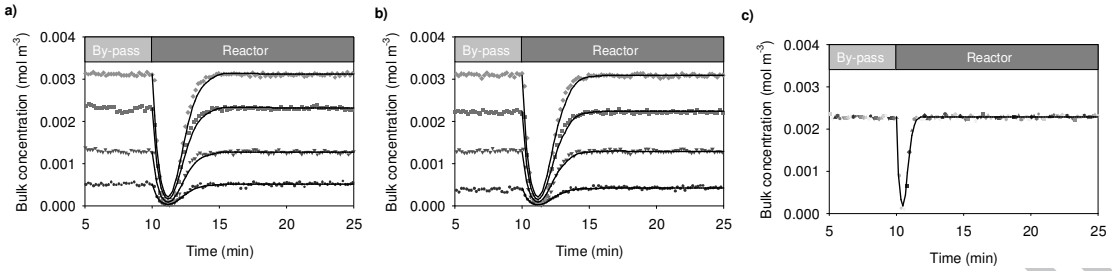

2

3

ACCEPTED MANUSCRIPT

1 **Figure 6 (print version)**

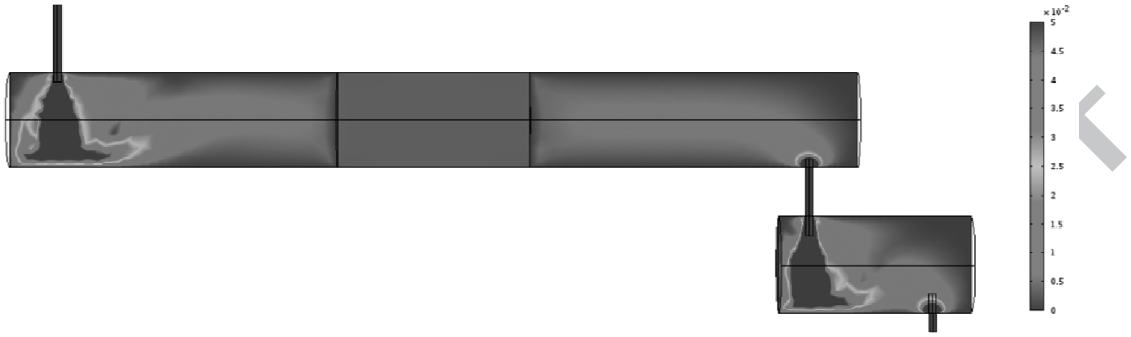

2
3

ACCEPTED MANUSCRIPT

ACCEPTED MANUSCRIPT

1 **Figure 7 (print version)**

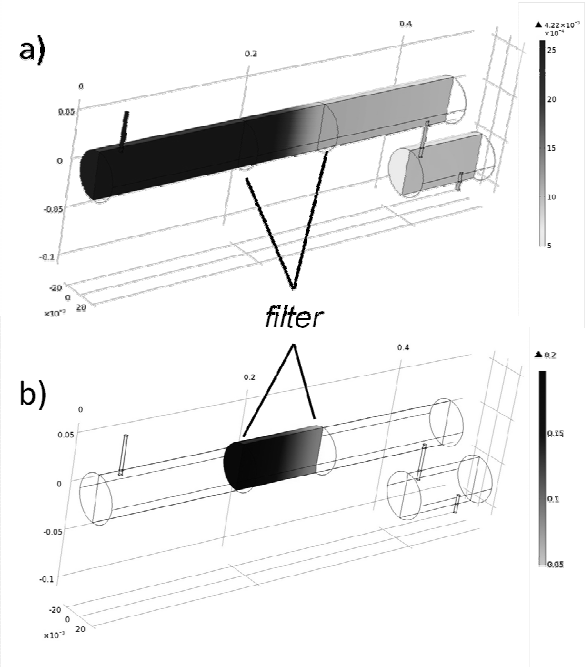

2

3

4

ACCEPTED MANUSCRIPT

ACCEPTED MANUSCRIPT

1 **Figure 8 (print version)**

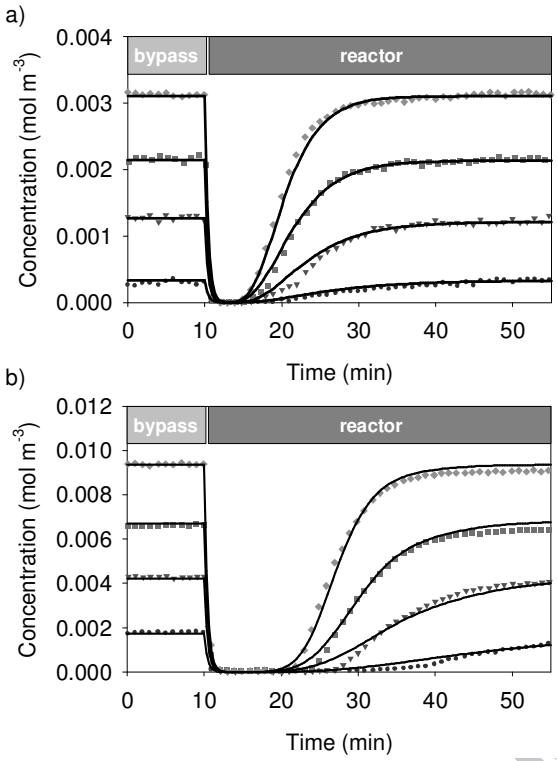

2

3

ACCEPTED MANUSCRIPT

ACCEPTED MANUSCRIPT

1 **Figure 9 (print version)**

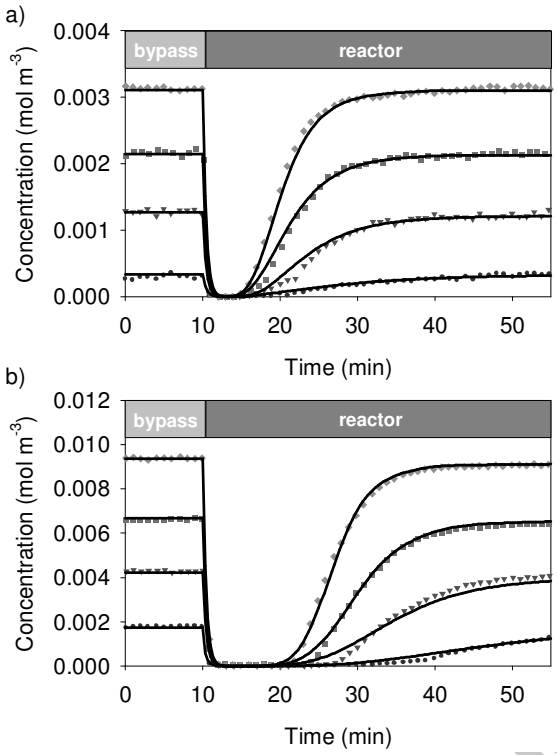

2

3

4

5

6

ACCEPTED MANUSCRIPT

ACCEPTED MANUSCRIPT

1 **Figure 10 (print version)**

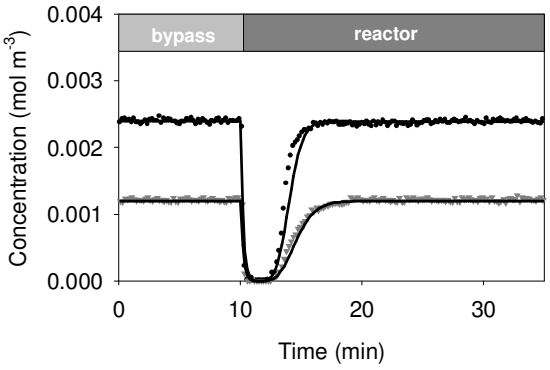

2

3

ACCEPTED MANUSCRIPT

1

2 Graphical abstract

3

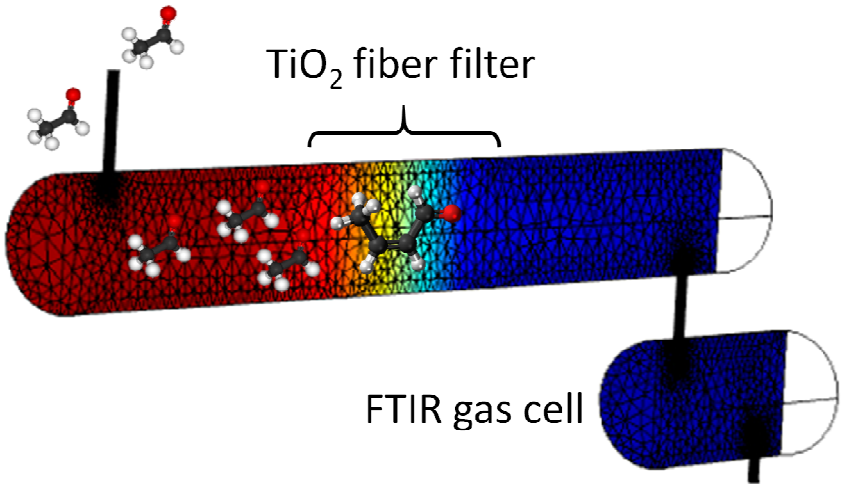

4

5

ACCEPTED MANUSCRIPT

ACCEPTED MANUSCRIPT

Research Highlights

- Acetaldehyde on TiO_2 adsorption parameters are accurately determined by CFD
- Not only steady-state but also transient adsorption behavior is modeled
- CFD enables to correct for air displacement effects in reactor and detector
- Inclusion of aldol surface condensation reaction further improves the model

ACCEPTED MANUSCRIPT